AGU PUBLICATIONS

Tectonics

RESEARCH ARTICLE
10.1002/2017TC004708

Special Section:
Orogenic cycles: From field observations to global geodynamics

Structural Geology and the Seismotectonics of the 2004 Great Sumatran Earthquake

G. S. Lister[1], M. A. Forster[1], J. E. Muston[1], S. Mousavi[1,2], and B. Hejrani[1,2]

[1]Structure Tectonics Team, Earth Dynamics Group, Research School of Earth Sciences, Australian National University, Canberra, Australia, [2]Now at Research School of Earth Sciences, The Australian National University, Canberra, Australia

Key Points:
- A tectonic mode switch that took place during an earthquake aftershock sequence
- Transforms that became normal faults and spreading centers that engaged in strike slip
- The megathrust slipped sideways into the gravitational potential well caused by prior slab rollback

Correspondence to:
G. S. Lister,
gordon.lister@anu.edu.au

Citation:
Lister, G. S., Forster, M. A., Muston, J. E., Mousavi, S., & Hejrani, B. (2018). Structural geology and the seismotectonics of the 2004 great Sumatran earthquake. *Tectonics*, *37*, 4101–4119. https://doi.org/10.1002/2017TC004708

Received 29 JUN 2017
Accepted 22 JAN 2018
Accepted article online 2 FEB 2018
Published online 5 NOV 2018

Abstract The paper sets out a method for structural analysis of seismotectonic data using centroid moment tensors and associated hypocenters from the Global Centroid Moment Tensor project, here illustrated for aftershocks from the 2004 great Sumatran earthquake. We show that the Sumatran segments of the megathrust were subject to compression in a direction near to orthogonal with the margin trend, consistent with the effect of relative movement of the adjacent tectonic plates. In contrast, the crust above the Andaman Sea segments was subject to margin-orthogonal extension, consistent with motion toward the gravitational potential well accumulated due to prior lateral (westward) rollback of the subducting edge of the northward moving Indian plate. Since this potential well is largely defined by topography, this episode of margin-orthogonal extension is at least in part "gravity driven." It did not last long. Within 15 months, an earthquake cluster across an Andaman Sea spreading segment showed a return to kinematics driven by relative plate motion. The transition can be explained if fluid activity temporarily reduced basal friction (or effective stress) but then led to healing so that the megathrust once again began to develop friction-locked segments. The influence of slab rollback is in developing a gravitational potential well facing the megathrust, hence drawing the overriding crust toward it in the immediate postrupture phase while the megathrust is in a weakened state. Plate tectonics dominates during interseismic gaps, once the megathrust heals, and regains frictional resistance.

Plain Language Summary The analysis of earthquake geology led to a discovery that stress states in the crust overlying the ruptured megathrust are transient, with a tectonic mode switch during the aftershock sequence. Contrary to what was expected, motion in the immediate aftermath of the great earthquake involved crust stretching and moving westward to fill the gravitational potential well caused by prior slab rollback, whereas within 15 months, with friction on the megathrust increasing, plate tectonics began once again to drive relative motion. Usually geologists and geophysicists think that the effects of slab rollback drive the kinematics of long-term motion, whereas earthquakes are almost always ascribed to the compression caused by plate tectonics. It is somewhat of a surprise to discover that things are in essence the other way around.

1. Introduction

The geological evolution of many orogenic terranes is dominated by the effects of tectonic mode switching: there are periods during the evolution of a mountain belt that witness extreme horizontal stretching, followed by periods of horizontal compression, and vice versa (Beltrando et al., 2008, 2010; Collins, 2002; Forster et al., 2004; Forster & Lister, 2008; Lister & Forster, 2009; Lister et al., 2001; Rawling & Lister, 2002; Viete et al., 2010; Wells et al., 2012). It is of interest why such tectonic mode switches occur and how abruptly they take place. Slab rollback may be the driver for periods of extreme extension in the lithosphere overriding and adjacent to a retreating subduction zone (Schellart & Lister, 2004; Schellart et al., 2006). Accretion events see terranes that first ram into each other, as the result of relative plate motion, and then accrete to the terrane stack in the over-riding plate, as the result of the formation of new thrusts that slice material from the subducting plate. During the act of accretion, the newly formed thrusts transfer tectonic slices to the terrane stack overriding the subduction zone. Transient increases in horizontal compressive stress may foreshadow individual accretion events, leading to episodes of overall crustal shortening in the orogenic belt. The transition from crustal shortening to extreme extension caused by renewed rollback after an accretion event may be the intrinsic underlying cause of episodicity during orogenesis (Lister et al., 2001).

The timescales involved in these processes are important: in particular, it is of interest to understand how slab rollback can drive extreme extension in the orogen core while ongoing convergence continues to be

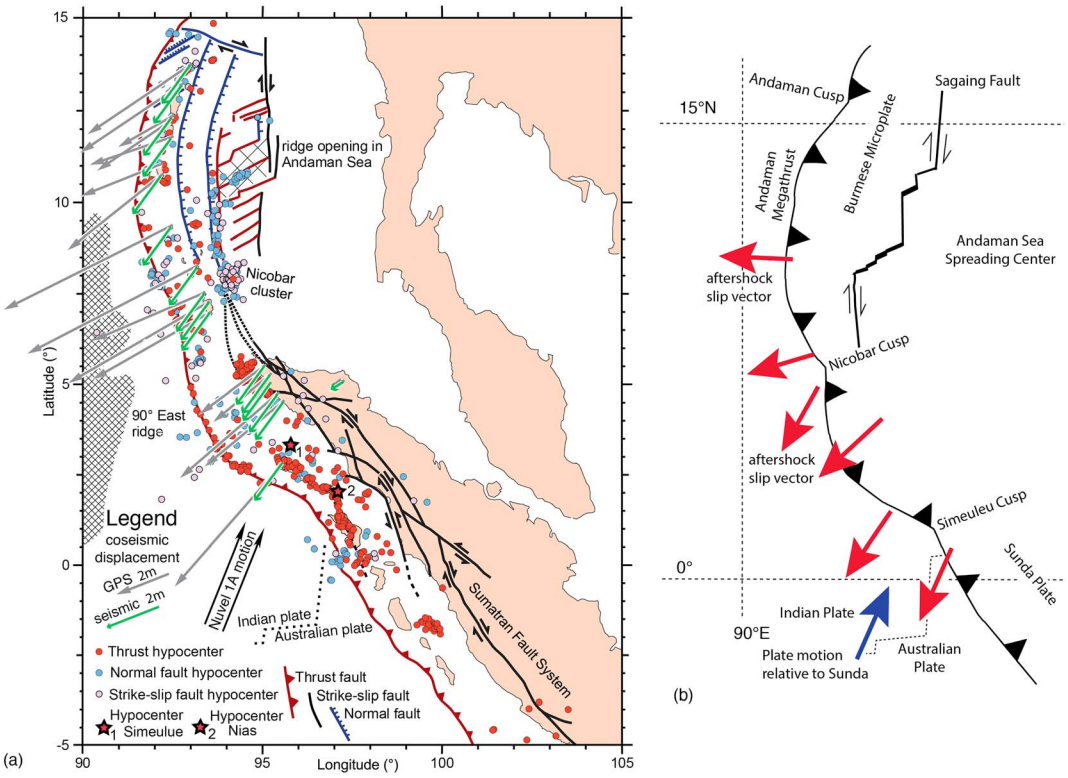

Figure 1. The *eQuakes* computer program allows automatic classification of earthquake kinematics, using information from an associated centroid moment tensor. Epicenters for thrusts are shown as red dots, while normal faults are blue, and strike-slip faults are shown with light mauve epicenters. (a) The seismogenic movement is shown (inferred by Ammon, 2005, and depicted by Chlieh et al., 2007), as well as GPS motions inferred from observations up to 30 days after the main shock (as depicted by Chlieh et al., 2007). (b) The morphotectonic elements of the Andaman segment are shown, with the Burmese microplate slipping on transforms separated by active oceanic spreading centers. This allows trends of slip vectors during and immediately subsequent to the main rupture to be contrasted with those inferred during the aftershock sequence.

accommodated by the basal megathrust. The lead up to an accretion event may be expressed in an individual episode of shortening that overall may last 2–3 Ma, but the eventual mode switch itself could be instantaneous. It is difficult to progress unless we gain insight as to the mechanisms that underlay geodynamics in the ancient Earth, at the times when individual tectonic mode switches took place. The uncertainties posed by ancient environments suggest we should look at relatively recent orogens to work out what causes tectonic mode switches, so as to determine the relevant aspects of their geodynamic evolution more accurately. We need to study places where the effect of relative plate motion can readily be distinguished from the effects of slab rollback, for example, in the European Alps, where extreme extension caused by westward rollback of the slab that once underlay the Palaeo-Po Basin can be distinguished from crustal shortening due to the continual northward motion of the Adria indentor. Similarly, while continued northward motion of the Indian plate drives the collision with Asia, westward rollback of the foundering eastern edge of the Indian plate drives ~E-W extension in the crust beneath the Andaman Sea, as evidenced by ~N-S normal faults (Figure 1a). In the overriding Burmese microplate (Figure 1b), ~E-W stretching would cause overall westward motion, with geometric incompatibilities accommodated by eastward steps of the bounding strike-slip faults and/or transforms. This brings into focus a modern tectonic dilemma: relative motion of microplates that is consistent with plate tectonics, while the obvious evidence for ongoing internal deformation denies the basic precept of "rigidity."

The theory of plate tectonics is based on geometric principles as apply to a planetary lithosphere defined by rigid (hence undeformable) tectonic plates. On a sphere, all relative motion of plates can be described by rigid-body rotations. The tectonic plates are not rigid, however, although their behavior is well approximated by considering them as stiff sheets of rock dominated by the elastic properties of the diffuse stress guides that occur at about the level of the brittle-to-ductile rheological transitions. The existence of these stress guides allows the transmission of deviatoric stress, even over long distances, so that plates move as an

entity, with a uniform motion determined by a torque balance that integrates the stresses caused by factors such as slab-pull, ridge push, and any basal tractions that apply. In sharp contrast, the orogenic processes that take place in adjacent mountain belts or sedimentary basins are governed by the rheology of an often weaker continental crust and motion of allochthonous sheets of rock directly driven by lateral variation in gravitational energy. In a slump sheet, on the small scale, the effect of topography is immediately evident. Motion is downslope. The drivers for movement on a larger scale are less obvious, yet topographic variation can drive coeval and coexisting zones of horizontal extension and linked horizontal shortening (e.g., Lagabrielle et al., 2010).

There has been a debate, which has lasted many decades, as to the relative merits of gravity-driven motion in mountain belts (i.e., gravity tectonics) versus motion solely as the result of relative plate motion (i.e., plate tectonics). There are many epithets given to the different manifestations of gravity-driven motion, including gravitational spreading, gravitational gliding, and gravitational slumping. The rheology involved is not simple. Ductile flow of rock depends on temporal as well as spatial scaling and on factors that localize motion at the base of an allochthon, that is, a sheet of rock that slides, such as a fold nappe or a thrust sheet. On the scale of an orogen, the motion of fold nappes and thrust sheets at the orogenic front can be argued to be coeval with uplift and ductile stretching in the orogen core (e.g., Rey et al., 2001). There is no need to demonstrate the existence of a continuous basal detachment linking foreland folding and thrusting with hinterland uplift and extension. Pervasive flow of rock within the orogen leads to the same outcome, that is, margin-orthogonal extension in the orogen core accommodated by coeval advance of the frontal megathrust.

The issue is that it is argued that the effects of rollback are on longer timescales than individual earthquakes, and textbooks invariably ascribe earthquakes to the effects of relative plate motion. However, here we demonstrate that the gravitational potential well caused by prior rollback may have driven motion during the aftershock sequence, immediately subsequent to the 2004 great Sumatran earthquake, which is not what should have been expected, even though motion due to the relative movement of the tectonic plates returned only after 15 months. This volume in honor of Marco Beltrando is the right place to first develop some basic principles that can be used for seismotectonic analysis based on centroid moment tensors to understand present day stress and strain distributions and then to explain interactions of gravity-driven tectonic processes within the earthquake cycle. Centroid moment tensor (CMT) data are from the Global CMT project (http://www.globalcmt.org/CMTsearch.html; Dziewonski et al., 1981; Ekström et al., 2012). This data, freely provided, enables research into the structural geology of earthquakes. Background images are Mercator projections from the Global Multiresolution Topography (GMRT) portal (Ryan et al., 2009; Smith, 1997; http://www.marine-geo.org/portals/gmrt/), which have been registered in the *eQuakes* program.

2. The 2004 Rupture of the Sumatran Megathrust

There are extensive reviews of the 2004 rupture of the Sumatran megathrust (e.g., Chlieh et al., 2007; Engdahl et al., 2007; Lay, 2005; Paul et al., 2012, 2014; Pesicek et al., 2010; Shearer & Bürgmann, 2010; Sibuet et al., 2007). Here we return to the recurring theme that the southern extent of the megathrust rupture behaved differently to that in the north but for different reasons than published previously. Epicenters for aftershocks up to 18 months after the 2004 great earthquake show distinct spatial groups of earthquakes, each associated with individual structures (Figure 1a). Figure 1b shows a map with morphotectonic elements.

The 2004 megathrust rupture first encapsulated the North Sumatran segment, defined by the geomorphic expression of the frontal megathrust between the Nicobar cusp and the Simeulue cusp (Figures 1b and 2a), with slip directions as shown (Figure 2b). The Andaman segment is defined by the geomorphic expression of the frontal megathrust between the Andaman cusp and the Nicobar cusp (Figures 1b and 2a), again with the spread of aftershock slip directions as shown (Figure 2b). There is significant variation in the dominant type of aftershock from north to south (Figure 3a), with compressional (thrust) earthquakes dominating in the south (in the North Sumatran segment) and extensional (normal) fault earthquakes dominating in the north (in the Andaman segment). Commensurate with this observation, Chlieh et al. (2007) noted coseismic uplift in the southern segment, with subsidence in the northern segment. Dilation (here interpreted to reflect coseismic crustal extension) in the Andaman segment was recorded by the GRACE satellite mission (Han et al., Han, 2006, Han et al., 2008).

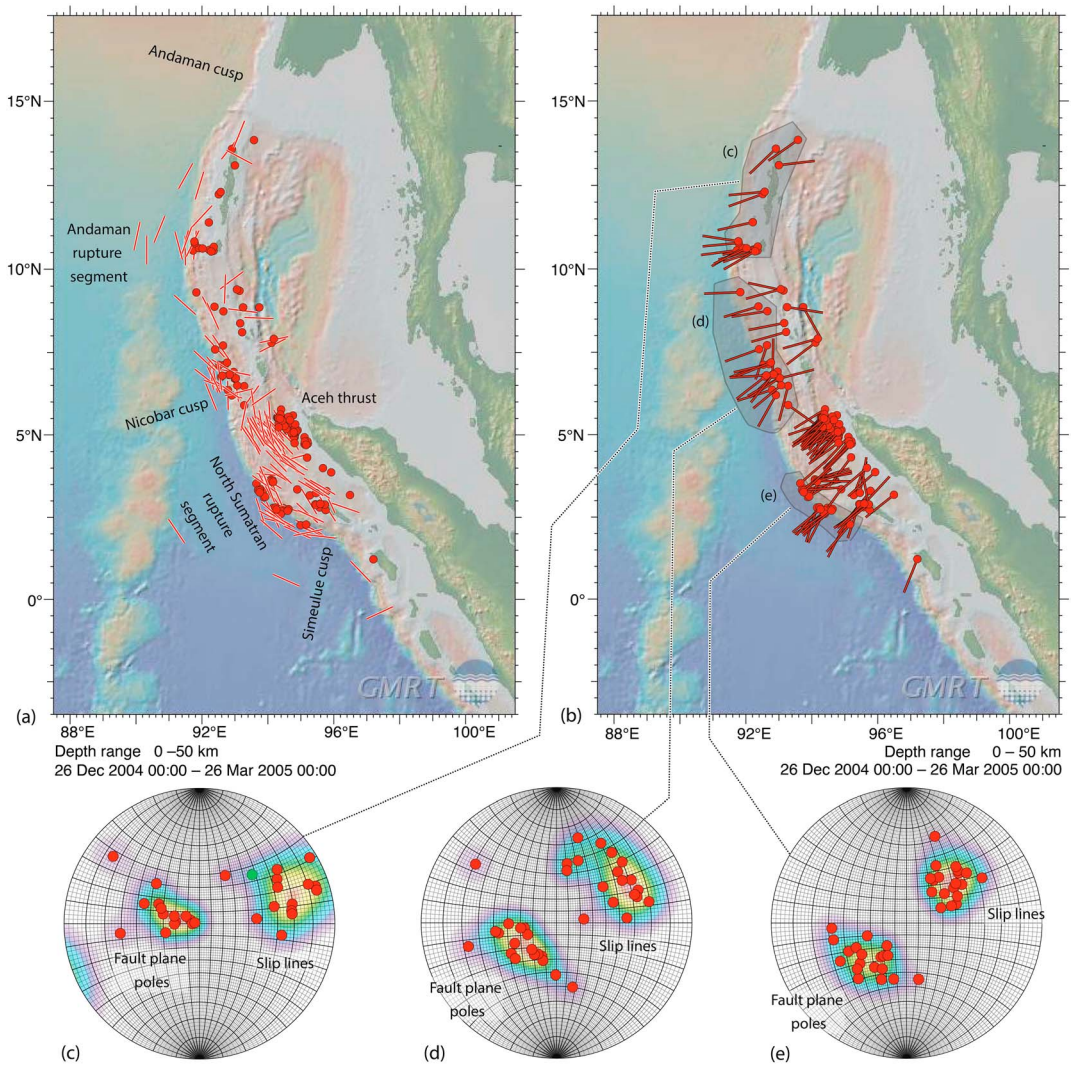

Figure 2. Epicenters for thrust aftershocks with hypocenters <50 km depth, from the Global CMT catalogue, for the first 3 months of the aftershock sequence. (a) Inferred strike, extrapolating the fault plane to the planet surface. (b) Slip-line trends and three spatial groups of aftershocks. Stereoplots show the orientation of slip lines for aftershocks with moment magnitude, $M_w \geq 5.5$: (c) slip is orthogonal to the margin; (d) slip is both orthogonal to the margin and to the direction of relative plate movement; and (e) slip takes place to the southeast, orthogonal to the margin, in the direction of relative plate movement. The scatter in Figure 2d suggests multislip, as do Kagan-Knopoff gamma factors.

The two types of megathrust operation are illustrated schematically in Figure 4. During the aftershock sequence, the Sumatran segment was dominated by horizontal compression, almost margin-orthogonal. The trend of slip directions on the bounding megathrust were parallel to the trend of motion on thrusts that splay from the megathrust in the internal parts of the overriding plate, with motion south-westward over adjacent fault blocks (Figure 2b). We refer to this behavior as that of a Mode I megathrust (Figure 4a). In contrast, during the aftershock sequence, the Andaman segment was dominated by margin-orthogonal extension, as evidenced by ~N-S normal faults (Figure 1a), although concurrent margin-orthogonal westward motion took place above the bounding megathrust (Figure 2b). We refer to this as Mode II megathrust behavior (Figure 4b). Cross sections (Figure 5) illustrating this contrasting behavior were constructed along the arcs shown in Figure 3a, using hypocenter data from Engdahl et al. (2007). Mode I megathrust operation involves overall shortening due to compression (with the axis of principal compressive stress horizontal), while Mode II megathrust operation involves horizontal extension (with the axis of principal compressive stress vertical). These contrasting movement patterns require a zone in which geometric incompatibilities are accommodated. It is thus of particular interest that, 32 days into the aftershock sequence, a swarm of earthquakes was triggered near the Nicobar Islands, where this tectonic mode switch occurs (Figure 1a).

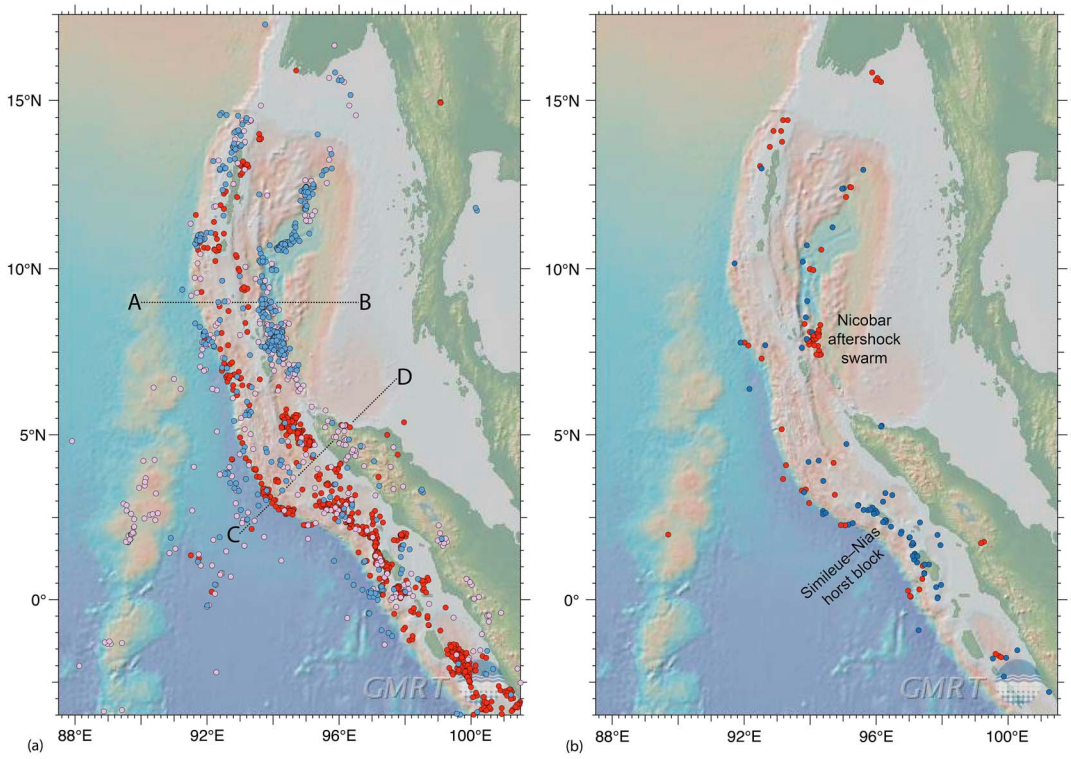

Figure 3. (a) *eQuakes* is used to classify 1,500 earthquakes with hypocenters <50 km depth, from the Global CMT catalogue, with all data from its inception until March 2017. Red circles are thrusts, blue circles are normal faults, and light mauve circles are strike-slip faults. (b) Epicenters for Kagan-Knopoff gamma factors, with (i) constrictive strain [0.75 to 1.00] (red circles); and (ii) flattening strain [−0.75 to −1.00] (dark blue circles). These deviations from plane strain may be related to extrinsic computational errors (e.g., in location or depth uncertainties), but they can also be the result of intrinsic features such as (i) simultaneous almost colinear slip on multiply oriented slip planes, with motion twisting so as to produce a constrictive moment; or (ii) cross-cutting slip planes with multiple slip directions extending the fault plane so as to produce a flattening moment.

Another fundamental distinction can be made between the northern and southern segments of the 2004 megathrust rupture. Movement directions have been estimated using GPS (Ammon, 2005; Banerjee et al., 2007; Chlieh et al., 2007; Jade et al., 2005; Paul et al., 2012, 2014; Rhie et al., 2007). In the south, the movement directions (plotted on Figure 1a from Chlieh et al., 2007) remained approximately collinear, whereas in the north, the GPS movement directions observed within 30 days of the main shock are rotated up to ~30° clockwise in comparison to the movement directions inferred by the analysis of seismic waves. This is of interest because the movement (Figure 1a) inferred from seismic waves (Ammon, 2005, as represented by Chlieh et al., 2007) occurs on a shorter timescale than GPS determinations made up to 30 days subsequent to the main shock. It appears that this rotation of the slip vector continues into the time of the aftershock sequence, since slip directions on the frontal megathrusts in the northern segments (Figure 1b) have rotated to be orthogonal to the margin trend and thus up to ~60° different in trend to the movement directions inferred during seismogenic slip. In sharp contrast to this behavior (above), the trend of slip directions in the compressional North Sumatran segment remained constant throughout the aftershock sequence.

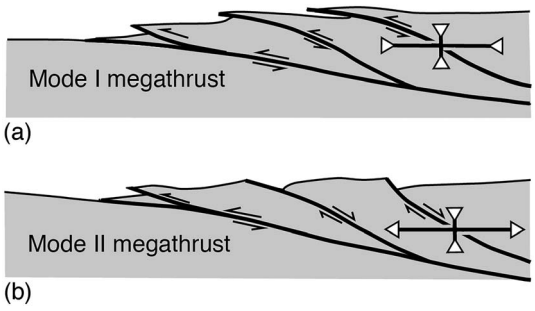

Figure 4. Cross sections with distinctly different geodynamic behaviors. In the south, offshore Sumatra, the crust is subject to margin orthogonal shortening. In the north (a) beneath the Andaman Sea, the crust is subject to margin-orthogonal extension, driven by gravitational collapse into the potential well caused by slab rollback. In the Andaman segment, a tectonic mode switch took place during the earthquake cycle. Motion at the start of the aftershock sequence involved normal faulting on transforms and strike-slip faulting near spreading centers. Once the switch took place, relative motion involved normal faulting near spreading centers.

3. Four Principles for Structural Analysis of Seismotectonic Data

To further analyze the aftershock pattern, we needed to analyze the movement picture for different spatial groups of earthquakes in

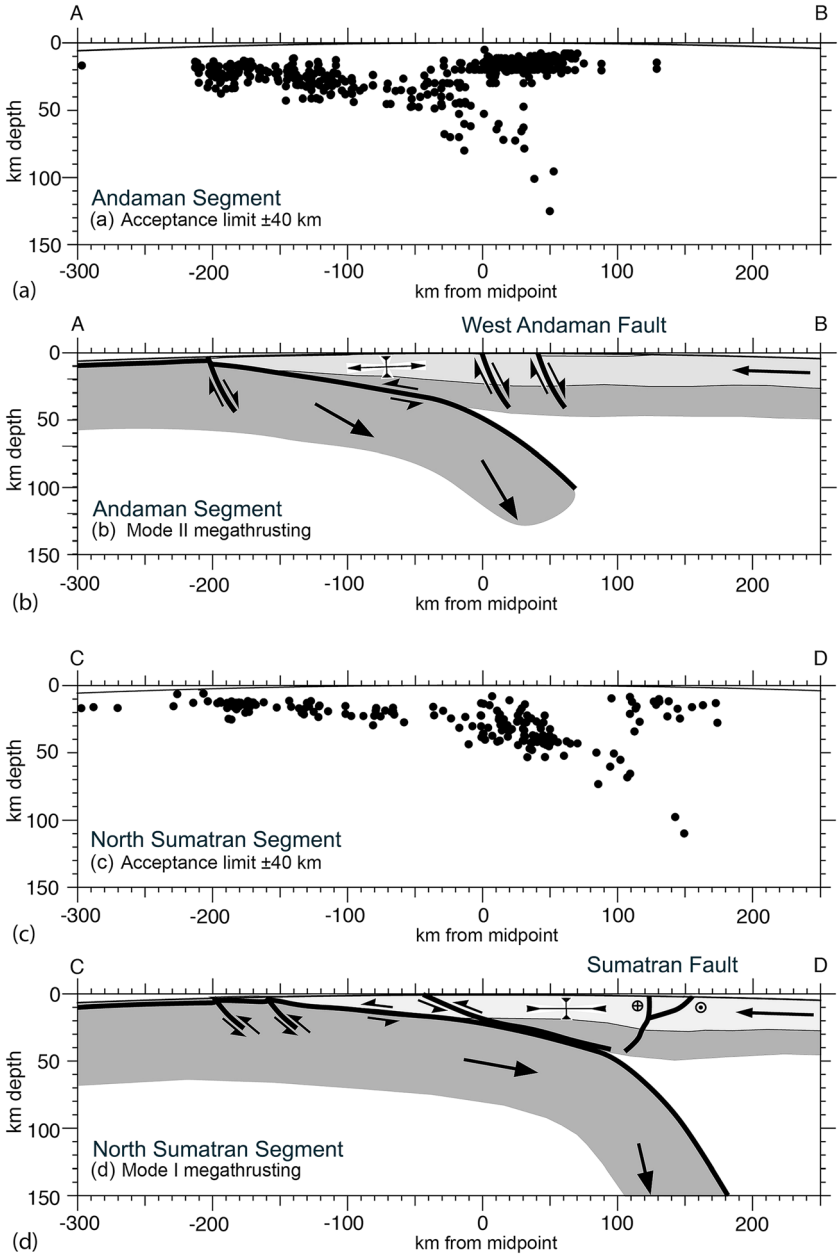

Figure 5. Cross sections produced by the *eQuakes* computer program along the lines of section shown in Figure 3a. (a, c) Hypocenters from Engdahl et al. (2007). (b, d) Interpreted cross sections show the main seismogenic structures that can be discerned in CMT data.

more detail: something not readily achieved using graphic representations such as beach balls, so the senior author decided (in the aftermath of the events of 2004) to write the computer program that is now known as *eQuakes*. It is intended to facilitate the application of the basic principles of structural geology to the analysis of movement pictures in an aftershock sequence, initially focused on extracting information from CMT data published in the Global CMT database (Dziewonski et al., 1981; Ekström et al., 2012). Data are analyzed ipso facto, with no attention paid to resolution or accuracy issues.

By using a stereoplot, the *eQuakes* program allows interactive classification of fault plane normals and slip-line directions extracted from centroid moment tensor data published by the Global CMT project (Dziewonski et al., 1981; Ekström et al., 2012). The first application of the program (in 2005) was to classify thrust fault earthquakes from the aftershock sequence (Figure 6), distinguishing two orientation groups: (i) the blue circles are poles to fault splays emanating from the basal megathrust, with corresponding slip-line

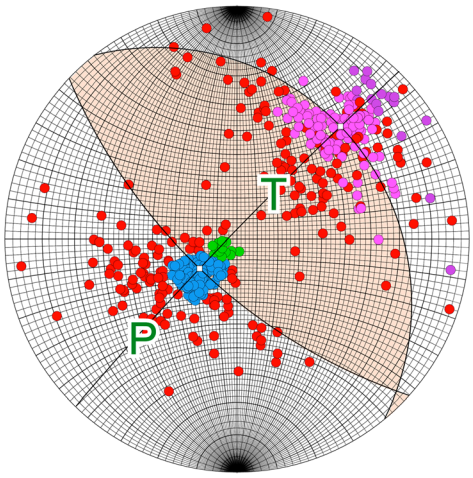

Figure 6. Thrust fault earthquakes from the aftershock sequence, classified using *eQuakes*, allowing distinction of two orientation groups: (i) poles to fault splays emanating from the basal megathrust (blue dots), with corresponding slip-line directions (magenta dots); and (ii) poles to aftershocks parallel to the basal megathrust (green dots), with slip lines (dark purple dots). There are numerous red dots representing slip lines and fault plane poles for thrust fault earthquakes that have not been classified. The beach ball, including its *P* and *T* axes, is for the first orientation group.

directions shown as magenta circles; and (ii) the green circle are poles to aftershocks parallel to the basal megathrust, with slip lines dark purple. It was thus possible to distinguish aftershocks taking place on the main rupture, as opposed to those taking place on splays emanating from it (Figure 6). There was no need to ascribe aftershocks to asperities on the megathrust, when individual seismogenic structures could be distinguished. In other words, the identification of orientation groups demonstrated that aftershocks take place on identifiable structures. This was the first principle reached in conducting this structural analysis, readily demonstrated using stereographic projections, or by precisely locating earthquake hypocenters (Dewey et al., 2007; Engdahl et al., 2007; Waldhauser et al., 2012).

3.1. Aftershocks Take Place on Identifiable Structures

A structural geologist will try to characterize seismogenic structures in terms of their geometry as well as their kinematics. Such information can be extracted from the centroid moment tensor, which has eigenvectors that describe the moment pulse emitted by the earthquake. The eigenvectors (i.e., the *P* and *T* axes) are not the axes of regional principal stress as often assumed—rather they describe the characteristic directions for the pulse of moment release, assumed to take place from a point in a continuum. The regional stress axes prior to the earthquake are sure to be different, as demonstrated by Lister et al. (2014). There will be coincidence only in the case that the rheology can be described as an isotropic perfectly plastic material (i.e., obeying the von Mises law of critical stress, $\tau \leq \tau_C$) or as an isotropic linearly viscous fluid. Even so, Lister et al. (2014) demonstrate that the orientation of the regional stress axes can be inferred from the kinematics involved in the pulse of moment release, either by assuming Coulomb-Mohr failure (for brittle cataclastic materials) or the Maximum Moment Principle (for semibrittle materials that exhibit ductile failure).

In an isotropic material, the moment pulse at a point can be described as a second rank tensor, with principal axes parallel to both the axes of the stress tensor and to the axes of the infinitesimal strain tensor associated with the deformation pulse. This isomorphism enables the moment tensor to be understood in terms of concomitant stress and strain pulses at the earthquake source. The moment tensor can be decomposed into the sum of a sequence of incremental plane strain deformations (Kagan, 1982; Kagan & Knopoff, 1985). It is then assumed that an individual plane-strain component results because of the simple shear deformation occasioned by an individual fault rupture, with the geometry of each slip system described by a fault plane normal and a slip-line direction. The von Mises strain condition is satisfied in that five linearly independent slip systems are sufficient to describe a general constant volume (isochoric) strain increment. The moment tensor can be generated by linear combination of the individual moment pulses associated with each slip system.

Difficulty arises when trying to go in reverse, inferring the movement pattern associated with a particular moment tensor. The same plane strain increment can be ascribed as the result of either of two complementary simple shear deformations—known as the conjugate fault plane solutions. The fault plane normal of one conjugate solution is the slip-line direction of the other, and the sense of shear of one is the opposite of the other conjugate solution. These two characteristic directions can be plotted: the standard seismological convention is to use the lower hemisphere of a stereographic projection. However, to classify one vector as a fault plane normal and, by implication, the other vector as the corresponding slip-line direction, additional information is necessary. This ambiguity must be resolved if we are to extract information in relation to fault kinematics.

3.2. Geology Allows Choice Between Conjugate Fault Plane Solutions

There are a number of ways in which a choice can be made between conjugate fault plane solutions, for example, by using directivity calculations (French et al., 2010; Warren & Shearer, 2006), or the H-C method

(Hejrani et al., 2010). However, in most cases, this level of sophistication is not necessary. In most cases, all that is necessary to classify fault plane poles versus slip-line directions can be provided using simple geological criteria: for example, thrusts have shallow dip, while normal faults have slip lines that typically dip ~60°. Strike-slip faults in most cases can be linked to geomorphic expressions of the effect of ongoing movement, similarly allowing resolution as to which conjugate solution should apply. Once points on a scatter diagram have been classified, they are of use in structural analysis, for example, allowing quantification of the kinematics of the seismogenic structures. This is the second principle achieved as the result of this analysis: bringing geology into the equation can allow the determination as to which of the two conjugate solutions expressed in any given CMT is applicable.

Caution needs to be adopted in taking this approach. Typically, the centroid moment tensor is calculated with zero trace. Seismologists ascribe the largest plane-strain component of the moment tensor to the effects of a double couple, and consider deviation as due to a non-double-couple compensated linear vector dipole component (Stierle et al., 2014; Vavryčuk, 2014). Once the non-double-couple component becomes significant, questions arise as to how to use the conjugate fault plane solutions listed in the seismic catalogues. There are significant non-double-couple components in many of the moment tensor solutions for this region (Figure 3b).

3.3. Aftershocks Are Kinematically Coordinated

The third principle achieved as the result of this analysis is that aftershocks are not random. The kinematic coordination of aftershocks was noted by Lister et al. (2008) in considering intermediate-depth earthquakes in a stretching and boudinaging slablet hanging down beneath the lithosphere of the Hindu Kush. It was recognized that the slip-line directions were steeply plunging and kinematically coordinated. This happened because a subducting slab was being stretched, with ductile failure (Lister et al., 2008) taking place on curvilinear fault planes. Relative motion (i.e., fault plane slip) was taking place in the same (or similar) directions. Kinematic coordination allows the definition of orientation groups, since earthquakes with similar slip directions, or similar fault plane normals, can be easily identified and grouped.

A group of earthquake ruptures inferred from an aftershock sequence can be considered as kinematically coordinated if either (or both) of the following condition(s) is(are) satisfied: (i) ruptures take place on the same (or similarly oriented) fault plane; or (ii) ruptures involve the same (or similarly oriented) slip-line direction. In the simplest case, rupture occurs on a single fault plane (or a set of parallel fault planes), and slip occurs toward the same direction. In this case, the stereoplot will display scatter about two single maxima, one maximum representing fault plane poles and the other the corresponding slip-line directions.

There are two very different scenarios that we should now consider, the first being multislip on a single fault plane, that is, simultaneous or sequential slip in many different directions on a single fault plane. The scatterplot may change fundamentally. One maximum (that representing the fault plane poles) will remain as would be expected, with uniform scatter. The other maximum may become elongate, with the plane of the elongation defining the trace of the fault plane on the stereonet. The second scenario involves the kinematic coordination offered by slip on many different fault planes (or on a curvilinear fault plane). This can create maxima with a different character. One maximum (that representing the kinematically coordinated slip-line direction) will remain, well-defined, with scatter uniformly around the maximum. There may be several other maxima on the scatterplot, each representing an individual fault plane orientation. Alternatively, the opposing maximum may be elongate, with the spread in orientation defining the extent of the continuous curvature on the fault plane.

Curved fault planes are common in geology, for example, in small-scale or large-scale boudinage structures caused by ductile faulting (Lister et al., 2008), but also in the flower geometries observed in brittle-fault splays emanating from basement-controlled wrench systems (Naylor et al., 1986). Such structures have been reported on strands of the Sumatran and West Andaman strike-slip faults (Martin et al., 2014; Wells et al., 2012), although their geometry is complicated by the effect of other factors. Multislip is also likely to be common, but there is little data to substantiate this claim. It would be useful if the centroid moment tensor contained information that allows distinction between multislip, or slip with curving slip-line directions, and slip with a single well-defined slip direction, but on curving fault planes, or fault plane segments.

3.4. Classification Using the Kagan-Knopoff Gamma Factor

The fourth principle achieved as the result of this analysis is a demonstration that it is possible to resolve the ambiguity present in scatterplots using the Kagan-Knopoff gamma factor (Kagan, 1982; Kagan & Knopoff, 1985). This is because a moment tensor with a significant non-double-couple component can involve the linear combination of two (or more) individual moment tensors, each caused by simultaneous faulting on independent (but adjacent) simultaneously operating fault ruptures. These two "slip systems" can be considered as defining basis vectors in a five-dimensional vector space, with a range of moment tensors resulting by varying the relative slip amount on each fault. There is no way around this ambiguity, and it points to a deficiency in terms of current practice in seismological catalogues in extracting a single double-couple component. The average can be reliably related to an individual basis vector, but only in the trivial case when the magnitude of slip on other simultaneously operating slip systems is insignificant. Otherwise there is ambiguity.

In the region examined here, more than 1,500 CMT solutions (Figure 3a) are recorded in the Global CMT database (from inception until March 2017). Less than half of the quakes examined had an absolute value of the gamma factor in the range [0–0.25], with about two thirds in the range [0–0.50]. A significant number (150) of the quakes examined had an absolute value of the gamma factor in the range [0.75–1.00], with epicenters as in Figure 3b. These quakes may well involve multislip, or slip on curved fault planes, so the choice of a single fault plane solution, or single slip-line direction, in such cases is misguided. There is no way to uniquely determine the decomposition of the moment tensor into a set of double-couple components.

We can proceed with an analysis if there is kinematic coordination, however, requiring at least one well-defined maximum on the scatterplot. In the case of slip involving curved fault planes and a twisting upward slip direction, the moment tensor that results will be in the constrictional field: most of the initial aftershocks in the Nicobar swarm fall into this category. This means that the single maximum in the orientation group represents a focused slip direction on curved fault planes, as expected in flower structures in strike-slip fault systems.

4. Spatial Clusters and Orientation Groups

There is a natural corollary to the principle that aftershocks on individual seismogenic structures (such as faults and/or ductile shear zones) should cluster in well-defined spatial groups. In the majority of cases, for any well-chosen spatial group of aftershocks, a set of orientation groups uniquely and simply describe the kinematics of the seismogenic structure(s). However, fault plane poles and/or slip-line directions distribute around single maxima in the scatterplot, so there can be "many to one" or "one to many" correlations between spatial groups and orientation groups.

Spatial clusters are evident throughout the aftershock sequence (e.g., Figure 2b), and the principle above can be illustrated in scatterplots for some of the individual spatial groups (Figures 2c, 2d, and 2e). Fault plane normals and slip-line directions are plotted on the lower hemisphere of a stereographic projection, for aftershocks $<$50 km depth, from the Global CMT catalogue, for the first 3 months of the aftershock sequence. Inferred strike is shown, using spherical trigonometry to project data to the surface (Figure 2a), with slip-line trends independently illustrated (Figure 2b). Slip on the megathrust north of the Nicobar Islands is orthogonal to the margin, while to the south, slip is parallel to the direction of relative plate movement. One spatial group, immediately north of the Nicobar cusp, captures these two slip directions (Figure 2d).

The case of a broadly defined spatial group defining one orientation group can be seen in the oceanic domain, which is marked by strike-slip faults and thrusts (Figure 3a). Sandiford et al. (2005) and Gordon and Houseman (2015) used geodynamic modeling to map the stress axes in this region. The orientation of the principal compressive stress is in a direction commensurate with Coulomb-Mohr failure on NNE-SSW trending left-lateral strike slip faults, and the trajectory of the deviatoric stress axes thus inferred is consistent with the trajectories inferred by Sandiford et al. (2005; their Figure 1C), but not with the World Stress Map (Heidbach et al., 2016), which mistakenly assumes that *P* axes define the orientation of principal compressive stress prior to failure. This part of the crust is under compression, with the axis of maximum compressive stress, σ_1, trending obliquely, but at a high angle, almost orthogonal, to the margin.

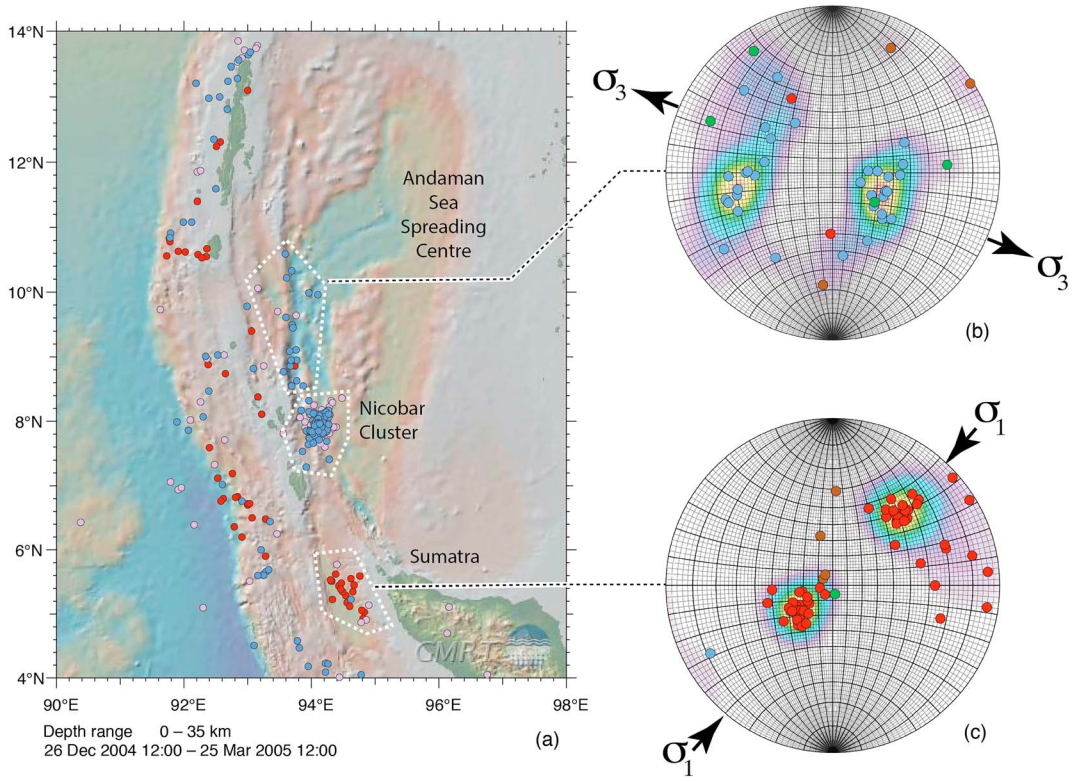

Figure 7. (a) Epicenters for earthquakes that initiated <35 km depth, from the Global CMT catalogue, for the first 3 months of the aftershock sequence: red, thrusts; blue, normal faults; light mauve, strike-slip faults. Stereoplots show the orientation of fault plane normals and slip lines for aftershocks: (b) down-dip slip on the east-dipping West Andaman Fault shows that this right-lateral transform has activated as a normal fault during the aftershock sequence; (c) slip lines for the ~30° northeast-dipping Aceh Thrust are updip, toward ~220°. The Andaman and North Sumatran segments thus each display a different tectonic mode.

The case of a correlation between a spatial group and a single orientation group is illustrated for the Aceh Thrust (Figures 7a and 7c), splays from which acted as distinct seismogenic structures accumulating numerous aftershocks (Waldhauser et al., 2012). A simple scatterplot of fault plane normals and slip-line directions is associated with this well-defined spatial group. Since these are thrust aftershocks, the scatterplot is readily classified, as shown. The fault plane dips on ~30° ENE, while fault slip takes place obliquely, toward ~220° (SW). The advantage of adopting a structural geology approach becomes obvious: instead of overlapping beach balls from which no statistical inference can be made, the scatterplot of fault plane normals and slip-line directions allows immediate quantitative recognition of the geometry of the seismogenic structure and its associated kinematics. Scatterplots of *P* axes and *T* axes associated with beach balls have little or no value in this aspect.

There are also orientation groups associated with individual seismogenic structures in the internal zone of the crust overriding the megathrust beneath the Andaman Sea. The most prominent of these is the right-lateral transform margin of the Andaman Sea spreading center, which during the aftershock period acted as an east-side down normal fault, dipping steeply east, striking north-south (cf. Figure 1 and Figures 7a and 7b). This requires the principal compressive stress, σ_1, to be vertical, while the least compressive stress, σ_3, trends approximately east-west, orthogonal to the strike of the outcrop of the frontal megathrust at the subducting margin, thus driving ~E-W trending horizontal extension. In comparison, offshore Sumatra, there is almost margin-orthogonal compression, with σ_1 horizontal, and trending ~NE-SW (Figures 7a and 7c).

5. Decomposition of a Complex Scatterplot

It is routinely possible to decompose a complex scatterplot into a finite set of orientation groups, as will now be demonstrated. The Nicobar cluster (Figure 1a) is a dense swarm of earthquakes that took place

beneath the Andaman Sea, northeast of the Nicobar Islands, 1 month into the aftershock sequence. The swarm continued for ~11 days, from 26 January 2005, rapidly decreasing in intensity toward the end of that period. Unlike most earthquake swarms, the Nicobar cluster was characterized by many shocks with moment magnitude exceeding 5. This meant that centroid moment tensor data could be determined and included in the Global CMT catalogue. These data in turn allow geometric analysis of the inferred fault plane motions.

The individual points on a scatterplot derived from CMT data can represent either a fault plane normal or slip-line directions. To resolve the ambiguity, each earthquake needs to be independently classified. This task is made easier if it is possible to define orientation groups that represent kinematically coordinated aftershocks, enabling an individual maximum on the scatterplot to be classified as a whole as either representing fault plane normals or slip-line directions. The first step is thus systematic decomposition of the scatterplot into orientation groups.

The input data are shown on a scatterplot of fault plane normals for the Nicobar Swarm (Figure 8a), classified as follows: (i) brown circles—poles to right-lateral strike-slip faults; (ii) green circles—poles to left-lateral strike-slip faults; (iii) red circle—a pole to a thrust or reverse fault; and (iv) blue circles—poles to normal faults. Each earthquake has two conjugate data points that plot orthogonally on the stereoplot. In the case of thrusts and normal faults, the conjugate solutions are usually of the same type, classified based on strike, dip, and rake (with 30° tolerances as shown). Therefore, the two circles shown for each earthquake are filled with the same color. In the case of strike-slip faults, the two conjugate solutions are distinguished with color based on the sense of shear. In the case that a fault is steep, with moderately plunging slip vectors, the conjugate solution will be classified as a thrust or as a normal fault and colored accordingly, but such circumstances arise only in exceptional cases.

Also note that a scatterplot showing fault-plane poles for both conjugate solutions is the same (within error) as what results when slip-line directions are plotted, because the slip line to one conjugate solution is the fault plane normal of the other. Again, solutions are colored based on the type of earthquake, with colors as described in the previous paragraph. Irrespective of whether the scatterplot shows slip-line directions or fault plane normals, the stereoplot allows choice of a specific conjugate solution and the opportunity to highlight its conjugate (Figure 8b).

On a map, the two conjugate solutions plot in the same place. On a stereoplot, they do not. Thus, the stereoplot offers a way to decompose a scatterplot into constituent orientation groups. All of the data points in an individual maximum can be selected (e.g., the yellow circles beneath the shaded polygon in Figure 8b), and the program is instructed to identify the conjugate solutions (here shown as light mauve circles). These conjugate solutions are then eliminated, thus making a (reversible) decision that an individual maximum is composed entirely of fault plane poles or slip-line directions. The relevant earthquakes are then identified, here as Orientation Group A and then also eliminated from the overall scatterplot. The residual scatterplot is then recontoured (Figure 8c), and data points in the next maximum are chosen. The conjugate solutions are once again identified and eliminated. This step may require two or more iterations, for example, in the case that a maximum is at the periphery (Figure 8c). The amalgamated collection of earthquakes is then identified, here as Orientation Group B, and again eliminated from the scatterplot. The residual scatterplot is recontoured, and the next maximum is selected. The conjugate solutions are identified (light mauve circles, Figure 8d) and then eliminated. The classified earthquakes are then amalgamated and identified, here as Orientation Group C. What remains is a pair of maxima, of which one is chosen, and the conjugates eliminated. The classified earthquakes are then once again amalgamated and identified, as here Orientation Group D. The process is now iterated to completion.

In the next step, the individual orientation groups are colored, to allow their ready distinction (Figure 9): red (Orientation Group A), green (Orientation Group B), magenta (Orientation Group C), and dark blue (Orientation Group D). The scatter diagram can show both fault plane poles and slip-line directions, for each orientation group (Figure 9), or a classification of individual maxima as either fault plane poles or slip-line directions (Figure 9b). The classification adopted (Figure 9b) implies the existence of multiple steeply dipping fault planes, consistent with Coulomb-Mohr failure as the result of ~NE-SW regional compression, as applies in the North Sumatran Domain.

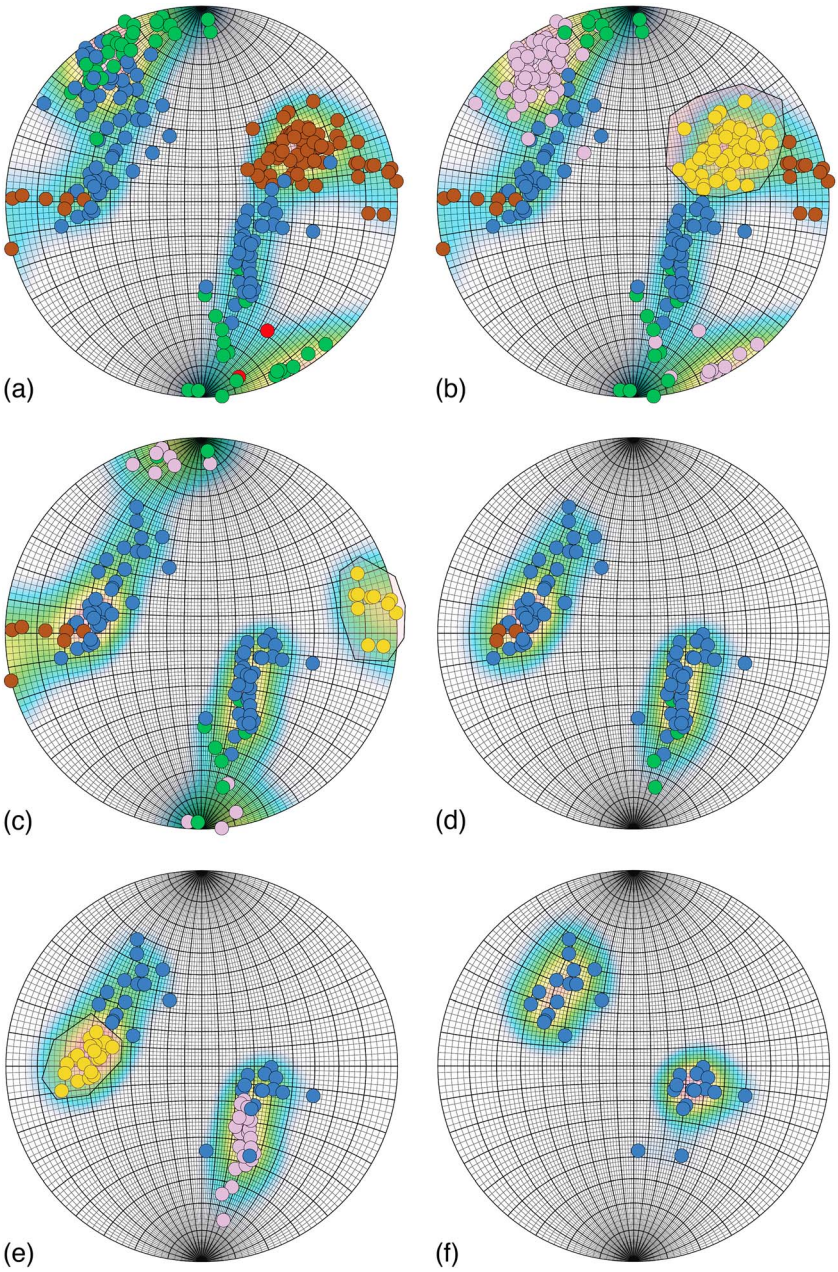

Figure 8. *eQuakes* has been used to decompose the complex scatterplot into four separate orientation groups (shown in Figure 9), by successive removal of individual maxima, and their associated conjugate solutions. Poles to thrust faults are shown in red, normal faults in blue, left-lateral strike-slip faults in green, and right-lateral strike-slip faults in brown. The individual steps in this process are discussed in the text, in detail. Data points in an individual maximum can be selected (yellow dots), and the data points representing the conjugate solutions are highlighted (light mauve dots).

Such a simple classification does not appear to be entirely correct, however, as detailed below. The next process to be undertaken involved examination of each orientation group (Figure 9a) in the context of the local geology (Figure 10), to see if arguments can be made that favor individual maxima as being classified as comprising fault plane normals versus slip-line directions, testing the interpretation shown (Figure 9b). In many cases, it was not possible to make an unambiguous classification. In the case of Orientation Group A, the strike-slip fault interpretation (Figure 9c) matches orientation groups formed in association with earthquakes on or near the Seulimeum Fault, further to the southeast. A ~N-S alignment of Orientation Group A epicenters (Figure 10) is subparallel to the Nicobar Fault and perhaps defines the termination of the

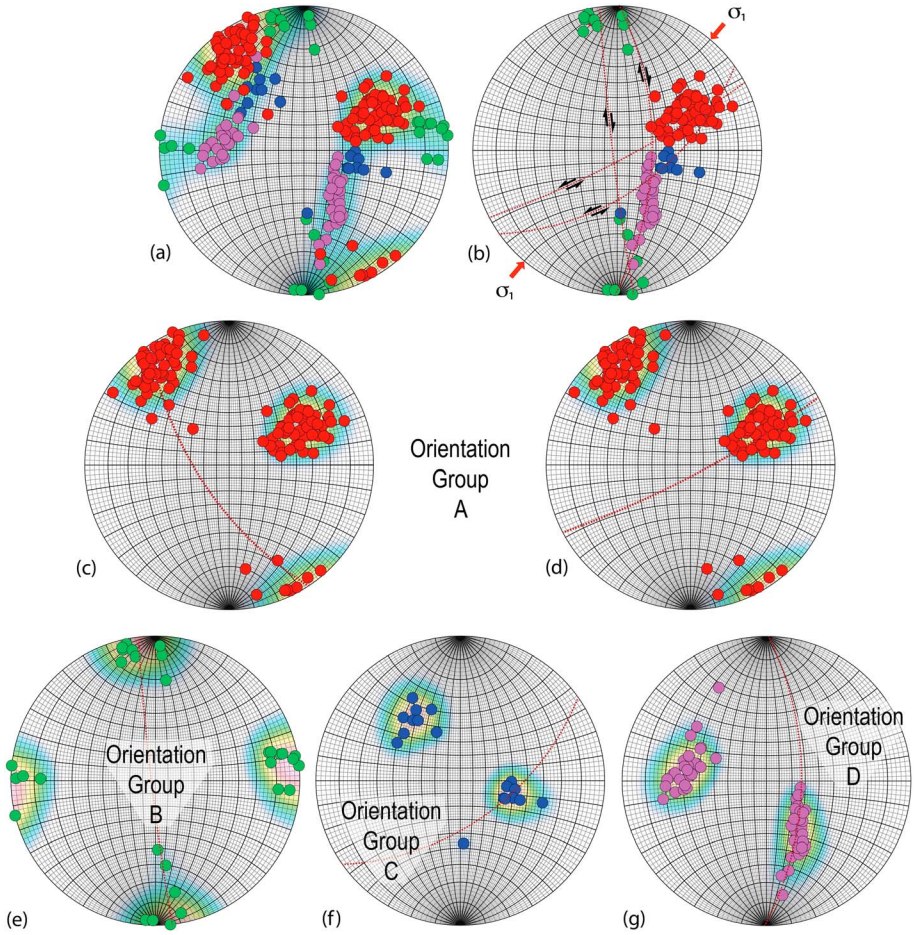

Figure 9. (a) The Nicobar swarm was decomposed by *eQuakes* into four separate orientation groups. (c, d) Orientation Group A has red dots, (e) while Orientation Group B has green dots, (f) C has dark blue dots, and (g) D has magenta dots. Orientation Group A has both conjugates active: (c) relating to strands of the Seulimeum wrench system (Figure 10); and (d) with oblique slip on a NNE-dipping normal fault. (e) Orientation Group B relates to the strike-slip Nicobar Fault (Figure 10). (f) Orientation Group C is a NE-dipping normal fault. (g) Orientation Group D has both conjugates active, with some multislip on a west-dipping fault (great circle as shown), but the majority involve reactivation of a north-dipping listric normal fault as left-lateral strike-slip faults, with a slip vector plunging ~30° westward.

Seulimeum Fault. Yet, as shown by superposed small circles on Figure 10, Orientation Group A also defines a ~WSW-ENE alignment parallel to bottom topography lineations that may reflect left-lateral strike-slip on normal faults formed in association with the Andaman Sea spreading centers. The latter alignment is subparallel to a slab tear that joins the Nicobar cusp (Kumar et al., 2016). Moreover, plotting the gamma factor in association with such an analysis shows that most aftershocks in Orientation Group A were constrictive and likely formed in association with flower structures at the termination of the Seulimeum Fault (cf. Weller et al., 2012). A significant subset of the aftershocks involved flattening, however, suggesting multislip on steeply dipping, ~WSW-ENE striking, normal faults. A valid conclusion is thus that both conjugate solutions in Orientation Group A were active (Figures 9c and 9d).

The same sort of analysis supports the choice of strike-slip solutions for Orientation Group B (Figure 9e) and the choice of normal fault solutions for Orientation Group C (Figure 9f). The sort of analysis applied to Orientation Group D is of particular interest, however, because gamma factors imply that the majority of aftershocks formed on cross-cutting curved fault planes that were nevertheless strongly kinematically coordinated, slipping toward a single direction that plunged ~30° westward. The remaining aftershocks could not be so-described, and these involved multislip on a ~N-S striking fault dipping steeply east. The geometry implies that this ~N-S striking fault was orthogonally cross-cut by curved faults that were north-facing listric faults. Maxima in the scatterplot for Orientation Group D can thus be reclassified to include both fault plane poles and slip lines.

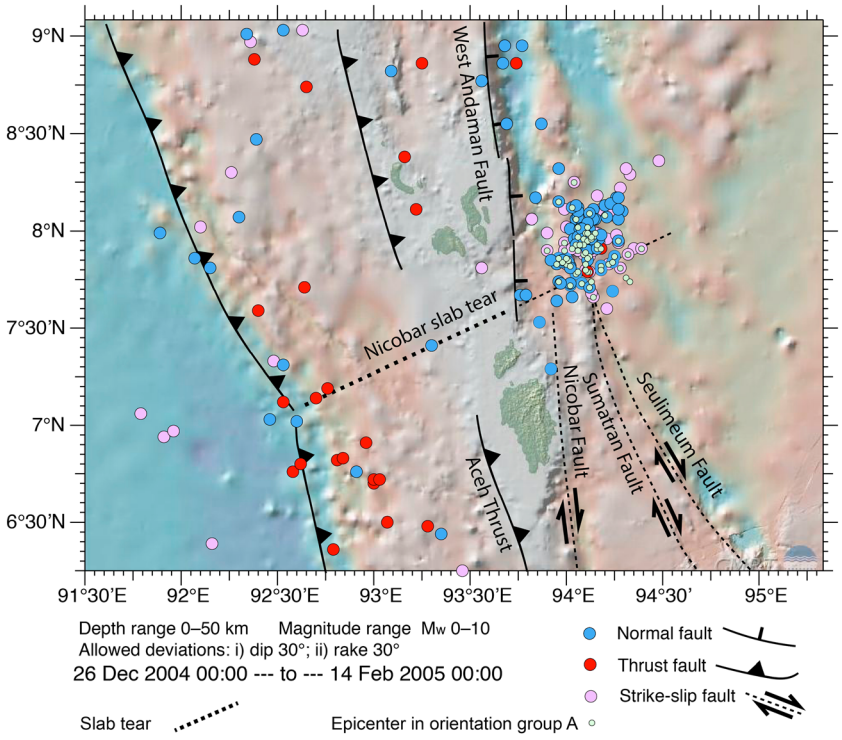

Figure 10. Map showing epicenters from the Nicobar swarm in the context of the local geology. Thrusts are shown as red dots, normal faults are blue, and strike slip faults are light mauve. The small light green dots mark epicenters from Orientation Group A. The trace of the slab tear inferred by Kumar et al. (2016) is also shown.

The geology suggests both northward continuation of the right lateral Sumatran Fault wrench system and the southward extension continuation of the West Andaman Fault as a right-lateral strike-slip fault system (Cattin et al., 2009; Chlieh et al., 2007; Cochran, 2010; Curray, 2005; Diehl et al., 2013; Kamesh Raju et al., 2004, 2007; Khan & Chakraborty, 2005; Mallick et al., 2017; Martin et al., 2014; McCaffrey, 1992, 2009; Moeremans & Singh, 2015). The orientation groups imply that strike-slip fault strands of the Sumatran Fault and Seulimeum Fault (Diehl et al., 2013) have intersected strands of the strike-slip Nicobar Fault (Figure 10) to form a strike-slip duplex (cf. Fernández-Blanco et al., 2016) and that geometric incompatibilities associated with sequential movements on these intersections explain the origin of the earthquake swarm.

The possible fault sets all involve a significant normal-slip component, suggesting transtensional movement consistent with the observation of narrow extensional basins (Diehl et al., 2013). There is no strike-slip component on the West Andaman Fault to the north of the Nicobar swarm, at this stage of the aftershock sequence. The structures to the north versus those to the south have different expressions and do not quite join up. Hence, we propose that the West Andaman Fault be named separately, restricted to refer to the structure to the north, where it appears as a steeply east dipping normal fault on the eastern flank of an elongate tilt block. In the south, there is a different structure, which we name the Nicobar strike-slip system (Figure 10).

It is also of interest that swarms of right-lateral strike-slip fault earthquakes took place in 2014, on prolongations of the Sumatran and Seulimeum Fault systems, allowing confirmation of the above movement picture and demonstrating that the same structures have remained active. Similar scatterplots result, and similar orientation groups emerge. Again, while the slip direction remained relatively constant, the fault planes fan from almost vertical to moderately dipping ~SW, as expected in a flower structure associated with a large wrench fault system. The trend of the slip direction is almost orthogonal to the trend of the Andaman Sea spreading centers, so this right-lateral displacement will assist with their continued dilation.

Overall, it appears that the Nicobar swarm developed because of different geometric incompatibilities: (i) in the south between the operation of intersecting right-lateral strike-slip fault systems; and (ii) in the north, in the Andaman segment, where preexisting transform faults reactivated as normal faults and pre-existing normal faults reactivated as left-lateral strike-slip structures. On the longer term, the existence of the

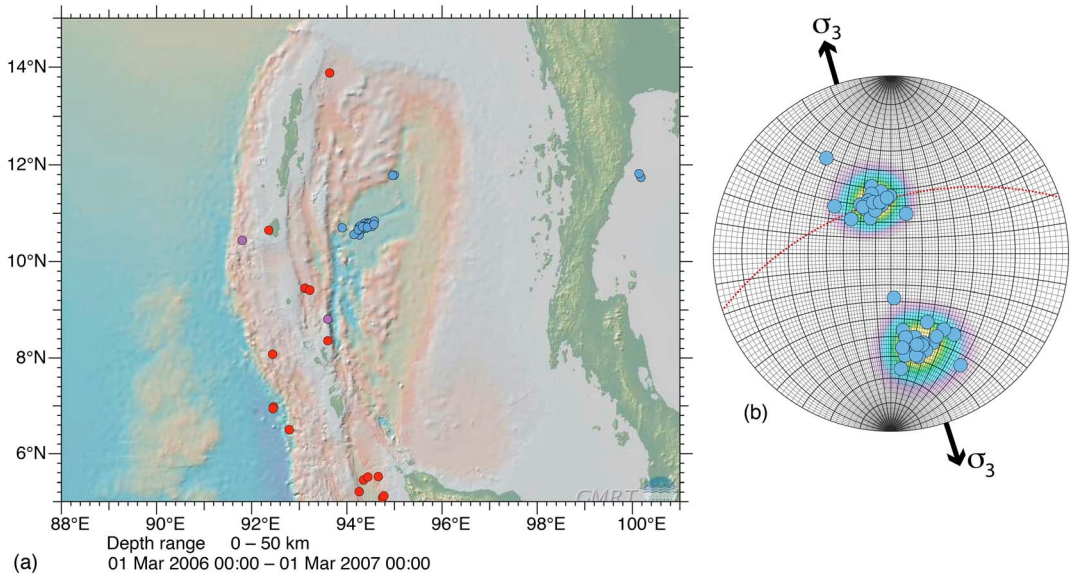

Figure 11. (a) A swarm of normal fault earthquakes on an Andaman Sea spreading center in March 2006 attests to a return to relative motion driven by plate tectonics. (b) The stereoplotshows slip lines scattered about the direction ~56° to >343°, consistent with a swarm developed on a normal fault, moderately dipping toward ~NNW.

transforms and the Andaman Sea spreading centers attest to the relative motion between the Burmese microplate and the Sunda Block driven by plate tectonics.

It is also likely that the Nicobar swarm occurred because fluid or volcanic activity locally decreased the effective stress, thus allowing failure conditions to be more readily achieved. There is however no evidence for this aspect in the moment tensor solutions. The non-double-couple component can be consistently and readily explained by the sum of moments caused by seismogenic multislip, either on one rupture plane, with similarly oriented slip directions, or on curved fault planes, with consistent slip directions. This is a disappointing conclusion in one aspect, for the geometry of the earthquake swarm is also of interest because it may provide some insight into the fluid-rock interactions that take place during the emplacement of porphyry and epithermal deposits in arc settings. Kamesh Raju et al. (2012) showed that the swarm localized on a dormant seamount and documented evidence for former hydrothermal activity and manganese nodules. Mukhopadhyay and Dasgupta (2008) and Mukhopadhyay et al. (2010) argued that the swarm demonstrated a complex faulting series with "initially ... strike-slip motion followed by normal faulting in repetitive sequences, whose representative fault planes orient at high angle to the regional faults." These authors suggest a nascent rift segment forming in a ~NW-SE trending direction and discuss a "pressure front from ascending magmatic fluid." Kundu et al. (2012) continue this discussion.

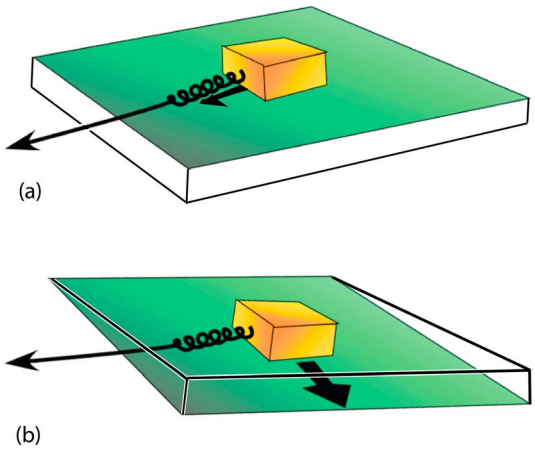

Figure 12. The effect of a gravitational potential well can be simply simulated by the motion of a friction block on a sloping surface. The dynamics are determined by basal friction, (a) with initial motion in the direction of the stretched spring and (b) motion thereafter determined by the balance of forces and how rapidly the reduced basal friction allows the friction block to slide downslope.

6. A Return to the Relative Motion of Microplates

A swarm of normal fault earthquakes took place on one of the Andaman Sea spreading centers (Figure 11a) in March 2006, attesting to a return to relative motion appropriate to the plate tectonic model for the region. The stereographic projection (Figure 11b) shows slip lines consistently dipping, scattered about a direction ~56° to >343°. There is no evidence for any magmatic influence on the moment tensor solutions. The data are consistent with a swarm developed on a single normal fault, moderately dipping ~NNW. The implication of this observation is that the state of stress has abruptly flipped, from margin-orthogonal extension in the immediate aftermath of the 2004 great earthquake, back to σ_3 with a ~NNW-SSE trending orientation.

7. Discussion and Conclusion

The state of stress varied remarkably over a short distance, from south to north, and with time. In the Andaman domain, the crust overriding the megathrust was stretched, orthogonal to the margin. To the south, offshore Sumatra, the crust overriding the megathrust is being shortened, in a direction close to the direction of relative plate motion. The Nicobar Swarm spatially separates these markedly different groups of aftershocks and marks the transition from transpressional wrenching in the Sumatran Fault system to transtensional wrenching implied by the geometry of the Andaman Sea spreading centers and their associated transform faults.

The cross section through the compressional North Sumatran segment (Figure 5b) shows the Sumatra Fault allowing partitioning of deformation as described by McCaffrey (1992, 2009). In contrast, the crust beneath the Andaman Sea (Figure 5a) was stretching horizontally and moving westward in what might be described as the results of a "rollback event." However, rollback is a longer-term process, creating the potential well westward of the megathrust and accounting for the slip deficit noted by Catherine et al. (2013). Anomalous subsidence rates recorded by tide gauges reflect this steady retreat. The rupture-triggered "rollback event" might therefore be better described as a "catchup process" as the overriding crust above the subduction zone surges westward, in a lithosphere-scale slump event, with ~E-W stretching of the crust east of the West Andaman Fault horizontally as the frontal megathrust advances.

The Nicobar swarm may have been facilitated by hydrothermal activity related to a seamount, or by magma intrusion. However, because the swarm is located where the transpressional regime of the Sumatran strike-slip fault system changes to that of the "microplate-bounding" transtensional wrench involved in the Andaman Sea spreading center, it may also be the result of the confluence of two tectonic modes of afterslip on the main rupture, with arc-normal compression to the south and arc-normal extension to the north. In any case, the orientation of stress trajectories is not static (cf. Heidbach et al., 2016) as implied by the concept of a World Stress Map. Our work shows that abrupt tectonic mode switches are possible, even within the duration of the earthquake cycle. A steady-state distribution of stress trajectories might be viewed as a long-term, plate-tectonic-driven state of affairs, but in the immediate aftermath of the 2004 great earthquake beneath the Andaman Sea, stress trajectories were rotated up to ~60° in consequence of gravity-driven motion of the crust toward the potential well caused by ongoing rollback of the transform margin of the Indian plate.

Temporal variation, with the orientation of the deviatoric stress axes in the crust beneath the Andaman Sea rotating ~60° clockwise after just under 15 months, demonstrates that the "catchup process" is a temporary event: a tectonic mode switch that has taken place within the timescale of an individual earthquake cycle. Orientation groups in the first year are consistent with margin orthogonal extension beneath the Andaman Sea (i.e., mode II megathrust behavior), whereas after that time, the pattern of deformation has reverted to that expected in consequence of relative plate motion, with the Andaman Sea transform faults once again moving as strike-slip faults and with ~NNW-SSE stretching across the Andaman Sea spreading centers, as consistent with their geometry and plate-tectonic significance. Down-dip slab tears required by the geometry of the subducting slab are consistent with those noted by Kumar et al. (2016). Slab tears enable retreat of individual segments and affect the overriding plate by allowing geodynamic uncoupling of different margin segments, as observed.

The swarm of aftershocks near the Nicobar Islands (Figure 1a), with both normal fault and strike-slip fault aftershocks (Figure 9b), appears to accommodate geometric mismatch between these Andaman and Sumatran domains. The Sumatran segment exhibited aftershock sequences consistent with ongoing Mode I megathrust behavior, while the Andaman segment exhibited aftershock sequences consistent with ongoing Mode II behavior. The Nicobar Aftershock Swarm marks the transition from one sort of slab dynamics to the other. In the longer term, effects related to the northward movement of India (driven by plate tectonics) cause motion on the Andaman Sea transforms and stretching across the Andaman Sea spreading centers. Such motion can be distinguished from the effects of westward rollback since ~E-W stretching causes the West Andaman Fault to act as an east-side down normal fault.

Textbooks attribute earthquakes in general to the effects of relative plate motion, that is, to plate tectonics. There has been some change in this perception. McKenzie and Jackson (2012) demonstrate gravitational

collapse of the accretionary prism during the 2011 Tohoku-oki great earthquake. In the case of the 2004 Great Sumatran Earthquake, the prior development of a gravitational potential well seaward of the outcrop of the bounding megathrust meant that during and after propagation of the initial rupture, there was an immediate tendency for relative motion to rotate clockwise, so as to become orthogonal to the margin. The rupturing of the boundary megathrust temporarily reduced frictional constraints, so that gravity began to drive motion on the ruptured megathrust and in the crust beneath the Andaman Sea during the early part of the aftershock sequence. This can be seen by comparing movement vectors inferred during propagation of the main rupture (Figure 1a; Ammon, 2005; Tsai et al., 2005; Rhie et al., 2007; depicted by Chlieh et al., 2007) and contrasting the change in trend with that of slip vectors observed during the aftershock sequence (Figure 1b). The motion of a simple friction block on a flat surface (Figure 12) illustrates the conceptual relation between slip driven by stored stress accumulated as the result of relative plate motion (Figure 12a), as opposed to slip on a weakened rupture responding dynamically to the existence of a gravitational potential well (Figure 12b). In the first case, when yield occurs (Figure 12a), motion takes place in the direction of the stretched spring. On a sloping surface, when yield occurs (Figure 12b), the reduced basal friction means that the dynamics of sliding downslope can dominate motion.

Acknowledgments

The combination of different data streams produces interesting results, as demonstrated in this collection of papers in honor of Marco Beltrando. He did his PhD here at ANU, with us, as part of our Structure-Tectonics team, in its early formative days, as the group reestablished itself after the move from Monash University to ANU. Marco's PhD was one of the first to emerge from our relocated group, focused on the enigmatic question as to how it is possible that extreme horizontal extension takes place during collisional orogeny. The authors acknowledge funding support from the Australian Research Council: Discovery Project DP120103554 "A unified model for the closure dynamics of ancient Tethys constrained by geodesy, structural geology, argon geochronology and tectonic reconstruction" and Linkage Project LP130100134 "Where to find giant porphyry and epithermal gold and copper deposits." The research was also supported by the "Satellites, Seismometers and Mass Spectrometers" initiative within the Research School of Earth Sciences at ANU. Bob Engdahl is thanked for his support during earlier versions and for providing data. An anonymous reviewer and Brian Wernicke considerably improved the manuscript. CMT data used in this paper can be downloaded from the Global CMT project (http://www.globalcmt.org/CMTsearch.html). Hypocenter data can be downloaded from the International Seismological Centre. The *eQuakes* program is available on the App Store. Background images are Mercator projections from the GMRT portal http://www.marine-geo.org/portals/gmrt/, registered using the *eQuakes* program.

References

Ammon, C. J. (2005). Rupture process of the 2004 Sumatra-Andaman earthquake. *Science*, *308*(5725), 1133–1139. https://doi.org/10.1126/science.1112260

Banerjee, P., Pollitz, F., Nagarajan, B., & Burgmann, R. (2007). Coseismic slip distributions of the 26 December 2004 Sumatra-Andaman and 28 March 2005 Nias earthquakes from GPS static offsets. *Bulletin of the Seismological Society of America*, *97*(1A), S86–S102. https://doi.org/10.1785/0120050609

Beltrando, M., Lister, G., Hermann, J., Forster, M., & Compagnoni, R. (2008). Deformation mode switches in the Penninic units of the Urtier Valley (western alps): Evidence for a dynamic orogen. *Journal of Structural Geology*, *30*(2), 194–219. https://doi.org/10.1016/j.jsg.2007.10.008

Beltrando, M., Lister, G. S., Rosenbaum, G., Richards, S., & Forster, M. A. (2010). Recognizing episodic lithospheric thinning along a convergent plate margin: The example of the early Oligocene alps. *Earth-Science Reviews*, *103*(3-4), 81–98. https://doi.org/10.1016/j.earscirev.2010.09.001

Catherine, J. K., Gahalaut, V. K., Srinivas, N., Kumar, S., & Nagarajan, B. (2013). Evidence of strain accumulation in the Andaman region for the giant 2004 Sumatra Andaman earthquake. *Bulletin of the Seismological Society of America*, *104*(1), 587–591.

Cattin, R., Chamot-Rooke, N., Pubellier, M., Rabaute, A., Delescluse, M., Vigny, C., et al. (2009). Stress change and effective friction coefficient along the Sumatra-Andaman-Sagaing fault system after the 26 December 2004 (M_w = 9.2) and the 28 March 2005 (M_w = 8.7) earthquakes. *Geochemistry, Geophysics, Geosystems*, *10*, Q03011. https://doi.org/10.1029/2008GC002167

Chlieh, M., Avouac, J. P., Hjorleifsdottir, V., Song, T. R. A., Ji, C., Sieh, K., et al. (2007). Coseismic slip and afterslip of the great M_w 9.15 Sumatra-Andaman earthquake of 2004. *Bulletin of the Seismological Society of America*, *97*(1A), S152–S173.

Cochran, J. R. (2010). Morphology and tectonics of the Andaman Forearc, northeastern Indian Ocean. *Geophysical Journal International*, *182*(2), 631–651. https://doi.org/10.1111/j.1365-246X.2010.04663.x

Collins, W. J. (2002). Hot orogens, tectonic switching, and creation of continental crust. *Geology*, *30*(6), 535. https://doi.org/10.1130/0091-7613(2002)030%3C0535:HOTSAC%3E2.0.CO;2

Curray, J. R. (2005). Tectonics and history of the Andaman Sea region. *Journal of Asian Earth Sciences*, *25*(1), 187–232. https://doi.org/10.1016/j.jseaes.2004.09.001

Dewey, J. W., Choy, G., Presgrave, B., Sipkin, S., Tarr, A. C., Benz, H., et al. (2007). Seismicity associated with the Sumatra-Andaman Islands earthquake of 26 December 2004. *Bulletin of the Seismological Society of America*, *97*(1A), S25–S42. https://doi.org/10.1785/0120050626

Diehl, T., Waldhauser, F., Cochran, J. R., Kamesh Raju, K. A., Seeber, L., Schaff, D., & Engdahl, E. R. (2013). Back-arc extension in the Andaman Sea: Tectonic and magmatic processes imaged by high-precision teleseismic double-difference earthquake relocation. *Journal of Geophysical Research: Solid Earth*, *118*, 2206–2224. https://doi.org/10.1002/jgrb.50192

Dziewonski, A. M., Chou, T.-A., & Woodhouse, J. H. (1981). Determination of earthquake source parameters from waveform data for studies of global and regional seismicity. *Journal of Geophysical Research - Solid Earth*, *86*(B4), 2825–2852. https://doi.org/10.1029/JB086iB04p02825

Ekström, G., Nettles, M., & Dziewonski, A. M. (2012). The global CMT project 2004–2010: Centroid-moment tensors for 13,017 earthquakes. *Physics of the Earth and Planetary Interiors*, *200-201*, 1–9. https://doi.org/10.1016/j.pepi.2012.04.002

Engdahl, E. R., Villasenor, A., DeShon, H. R., & Thurber, C. H. (2007). Teleseismic relocation and assessment of seismicity (1918-2005) in the region of the 2004 M_w 9.0 Sumatra-Andaman and 2005 M_w 8.6 Nias Island Great earthquakes. *Bulletin of the Seismological Society of America*, *97*(1A), S43–S61. https://doi.org/10.1785/0120050614

Fernández-Blanco, D., Philippon, M., & von Hagke, C. (2016). Structure and kinematics of the Sumatran fault system in North Sumatra (Indonesia). *Tectonophysics*, *693*, 453–464. https://doi.org/10.1016/j.tecto.2016.04.050

Forster, M., Lister, G., Compagnoni, R., Giles, D., Hills, Q., Betts, P., et al. (2004). Mapping of oceanic crust with "HP" to "UHP" metamorphism: The Lago di Cignana Unit, (Western Alps). In G. Pasquarè & C. Venturini (Eds.), *Mapping geology in Italy* (pp. 279–288). Firenze: S.EL.CA.

Forster, M. A., & Lister, G. S. (2008). Tectonic sequence diagrams and the structural evolution of schists and gneisses in multiply deformed terranes. *Journal of the Geological Society*, *165*(5), 923–939. https://doi.org/10.1144/0016-76492007-016

French, S. W., Warren, L. M., Fischer, K. M., Abers, G. A., Strauch, W., Protti, J. M., & Gonzalez, V. (2010). Constraints on upper plate deformation in the Nicaraguan subduction zone from earthquake relocation and directivity analysis. *Geochemistry, Geophysics, Geosystems*, *11*, Q03S20. https://doi.org/10.1029/2009GC002841

Gordon, R. G., & Houseman, G. A. (2015). Deformation of Indian Ocean lithosphere: Evidence for a highly nonlinear rheological law. *Journal of Geophysical Research: Solid Earth*, *120*, 4434–4449. https://doi.org/10.1002/2015JB011993

Han, S. C. (2006). Crustal dilatation observed by GRACE After the 2004 Sumatra-Andaman earthquake. *Science*, *313*(5787), 658–662. https://doi.org/10.1126/science.1128661

Han, S.-C., Sauber, J., Luthcke, S. B., Ji, C., & Pollitz, F. F. (2008). Implications of postseismic gravity change following the great 2004 Sumatra-Andaman earthquake from the regional harmonic analysis of GRACE intersatellite tracking data. *Journal of Geophysical Research*, *113*, B11413. https://doi.org/10.1029/2008JB005705

Heidbach, O., Rajabi, M., Reiter, K., & Ziegler, M. (2016). World stress map 2016. *GFZ Data Service*. https://doi.org/10.5880/WSM.2016.002

Hejrani, B., Hatami, M. R., & Mousavi, S. (2010). Fault-plane identification by a geometrical method – Application to moderate earthquake M_w 5.1 Kerman, Iran, 72nd EAGE Conference and Exhibition.

Jade, S., Ananda, M., Kumar, P., & Banerjee, S. (2005). Co-seismic and post-seismic displacements in Andaman and Nicobar islands from GPS measurements. *Current Science*, *88*, 1980–1984.

Kagan, Y. Y. (1982). Stochastic model of earthquake fault geometry. *Geophysical Journal International*, *71*(3), 659–691. https://doi.org/10.1111/j.1365-246X.1982.tb02791.x

Kagan, Y. Y., & Knopoff, L. (1985). The first-order statistical moment of the seismic moment tensor. *Geophysical Journal International*, *81*(2), 429–444. https://doi.org/10.1111/j.1365-246X.1985.tb06411.x

Kamesh Raju, K. A., Murty, G. P. S., Amarnath, D., & Kumar, M. L. M. (2007). The West Andaman fault and its influence on the aftershock pattern of the recent megathrust earthquakes in the Andaman-Sumatra region. *Geophysical Research Letters*, *34*, L03305. https://doi.org/10.1029/2006GL028730

Kamesh Raju, K. A., Ramprasad, T., Rao, P. S., Ramalingeswara Rao, B., & Varghese, J. (2004). New insights into the tectonic evolution of the Andaman basin, northeast Indian Ocean. *Earth and Planetary Science Letters*, *221*(1-4), 145–162. https://doi.org/10.1016/S0012-821X(04)00075-5

Kamesh Raju, K. A., Ray, D., Mudholkar, A., Murty, G. P. S., Gahalaut, V. K., Samudrala, K., et al. (2012). Tectonic and volcanic implications of a cratered seamount off Nicobar Island, Andaman Sea. *Journal of Asian Earth Sciences*, *56*, 42–53. https://doi.org/10.1016/j.jseaes.2012.04.018

Khan, P. K., & Chakraborty, P. P. (2005). Two-phase opening of Andaman Sea: A new seismotectonic insight. *Earth and Planetary Science Letters*, *229*(3-4), 259–271. https://doi.org/10.1016/j.epsl.2004.11.010

Kumar, P., Srijayanthi, G., & Ravi Kumar, M. (2016). Seismic evidence for tearing in the subducting Indian slab beneath the Andaman arc. *Geophysical Research Letters*, *43*, 4899–4904. https://doi.org/10.1002/2016GL068590

Kundu, B., Legrand, D., Gahalaut, K., Gahalaut, V. K., Mahesh, P., Kamesh Raju, K. A., et al. (2012). The 2005 volcano-tectonic earthquake swarm in the Andaman Sea: Triggered by the 2004 great Sumatra-Andaman earthquake. *Tectonics*, *31*, TC5009. https://doi.org/10.1029/2012TC003138

Lagabrielle, Y., Labaume, P., & de Saint Blanquat, M. (2010). mantle exhumation, crustal denudation, and gravity tectonics during Cretaceous rifting in the Pyrenean realm (SW Europe): Insights from the geological setting of the lherzolite bodies. *Tectonics*, *29*, TC4012. https://doi.org/10.1029/2009TC002588

Lay, T. (2005). The great Sumatra-Andaman earthquake of 26 December 2004. *Science*, *308*(5725), 1127–1133. https://doi.org/10.1126/science.1112250

Lister, G., & Forster, M. (2009). Tectonic mode switches and the nature of orogenesis. *Lithos*, *113*(1-2), 274–291. https://doi.org/10.1016/j.lithos.2008.10.024

Lister, G., Kennett, B., Richards, S., & Forster, M. (2008). Boudinage of a stretching slablet implicated in earthquakes beneath the Hindu Kush. *Nature Geoscience*, *1*(3), 196–201. https://doi.org/10.1038/ngeo132

Lister, G. S., Forster, M. A., & Rawling, T. J. (2001). Episodicity during orogenesis. *Geological Society, London, Special Publications*, *184*(1), 89–113. https://doi.org/10.1144/GSL.SP.2001.184.01.06

Lister, G. S., Tkalčić, H., McClusky, S., & Forster, M. A. (2014). Skewed orientation groups in scatter plots of earthquake fault plane solutions: Implications for extensional geometry at oceanic spreading centers. *Journal of Geophysical Research: Solid Earth*, *119*, 2055–2067. https://doi.org/10.1002/2013JB010706

Mallick, R., Parameswaran, R. M., & Rajendran, K. (2017). The 2005 and 2010 earthquakes on the Sumatra–Andaman trench: Evidence for post-2004 megathrust intraplate rejuvenation. *Bulletin of the Seismological Society of America*. https://doi.org/10.1785/0120160147

Martin, K. M., Gulick, S. P. S., Austin, J. A., Berglar, K., Franke, D., & Udrekh (2014). The West Andaman fault: A complex strain-partitioning boundary at the seaward edge of the Aceh Basin, offshore Sumatra. *Tectonics*, *33*, 786–806. https://doi.org/10.1002/2013TC003475

McCaffrey, R. (1992). Oblique plate convergence, slip vectors, and forearc deformation. *Journal of Geophysical Research*, *97*(B6), 8905. https://doi.org/10.1029/92JB00483

McCaffrey, R. (2009). The tectonic framework of the Sumatran subduction zone. *Annual Review of Earth and Planetary Sciences*, *37*(1), 345–366. https://doi.org/10.1146/annurev.earth.031208.100212

McKenzie, D., & Jackson, J. (2012). Tsunami earthquake generation by the release of gravitational potential energy. *Earth and Planetary Science Letters*, *345-348*, 1–8. https://doi.org/10.1016/j.epsl.2012.06.036

Moeremans, R. E., & Singh, S. C. (2015). Fore-arc basin deformation in the Andaman-Nicobar segment of the Sumatra-Andaman subduction zone: Insight from high-resolution seismic reflection data. *Tectonics*, *34*, 1736–1750. https://doi.org/10.1002/2015TC003901

Mukhopadhyay, B., Acharyya, A., Mukhopadhyay, M., & Dasgupta, S. (2010). Relationship between earthquake swarm, rifting history, magmatism and pore pressure diffusion — An example from South Andaman Sea, India. *Journal of the Geological Society of India*, *76*(2), 164–170.

Mukhopadhyay, B., & Dasgupta, S. (2008). Swarms in Andaman Sea, India — A seismotectonic analysis. *Acta Geophysica*, *56*(4). https://doi.org/10.2478/s11600-008-0039-5

Naylor, M. A., Mandl, G., & Supesteijn, C. H. K. (1986). Fault geometries in basement-induced wrench faulting under different initial stress states. *Journal of Structural Geology*, *8*(7), 737–752. https://doi.org/10.1016/0191-8141(86)90022-2

Paul, J., Rajendran, C. P., Lowry, A. R., Andrade, V., & Rajendran, K. (2012). Andaman postseismic deformation observations: Still slipping after all these years? *Bulletin of the Seismological Society of America*, *102*(1), 343–351. https://doi.org/10.1785/0120110074

Paul, J., Rajendran, K., & Rajendran, C. P. (2014). Slow slip acceleration beneath Andaman Islands triggered by the 11 April 2012 Indian Ocean earthquakes. *Bulletin of the Seismological Society of America*, *104*(3), 1556–1561. https://doi.org/10.1785/0120130220

Pesicek, J. D., Thurber, C. H., Zhang, H., DeShon, H. R., Engdahl, E. R., & Widiyantoro, S. (2010). Teleseismic double-difference relocation of earthquakes along the Sumatra-Andaman subduction zone using a 3-D model. *Journal of Geophysical Research*, *115*, B10303. https://doi.org/10.1029/2010JB007443

Rawling, T. J., & Lister, G. S. (2002). Large-scale structure of the eclogite–blueschist belt of New Caledonia. *Journal of Structural Geology*, *24*(8), 1239–1258. https://doi.org/10.1016/S0191-8141(01)00128-6

Rey, P., Vanderhaeghe, O., & Teyssier, C. (2001). Gravitational collapse of the continental crust: Definition, regimes and modes. *Tectonophysics*, *342*(3-4), 435–449. https://doi.org/10.1016/S0040-1951(01)00174-3

Rhie, J., Dreger, D., Burgmann, R., & Romanowicz, B. (2007). Slip of the 2004 Sumatra-Andaman earthquake from joint inversion of long-period global seismic waveforms and GPS static offsets. *Bulletin of the Seismological Society of America*, *97*(1A), S115–S127. https://doi.org/10.1785/0120050620

Ryan, W. B. F., Carbotte, S. M., Coplan, J. O., O'Hara, S., Melkonian, A., Arko, R., et al. (2009). Global Multi-Resolution Topography (GMRT) synthesis data set. *Geochemistry, Geophysics, Geosystems*, *10*, Q03014. https://doi.org/10.1029/2008GC002332

Sandiford, M., Coblentz, D., & Schellart, W. P. (2005). Evaluating slab-plate coupling in the Indo-Australian plate. *Geology*, *33*(2), 113. https://doi.org/10.1130/G20898.1

Schellart, W. P., & Lister G. S. (2004). Tectonic models for the formation of arc-shaped convergent zones and backarc basins, in *Geological Society of America Special Paper 383: Orogenic curvature: Integrating paleomagnetic and structural analyses*, edited, Geological Society of America, Boulder, CO, pp. 237–258.

Schellart, W. P., Lister, G. S., & Toy, V. G. (2006). A Late Cretaceous and Cenozoic reconstruction of the Southwest Pacific region: Tectonics controlled by subduction and slab rollback processes. *Earth-Science Reviews*, *76*(3-4), 191–233. https://doi.org/10.1016/j.earscirev.2006.01.002

Shearer, P., & Bürgmann, R. (2010). Lessons learned from the 2004 Sumatra-Andaman megathrust rupture. *Annual Review of Earth and Planetary Sciences*, *38*(1), 103–131. https://doi.org/10.1146/annurev-earth-040809-152537

Sibuet, J., Rangin, C., Lepichon, X., Singh, S., Cattaneo, A., Graindorge, D., et al. (2007). 26th December 2004 great Sumatra–Andaman earthquake: Co-seismic and post-seismic motions in northern Sumatra. *Earth and Planetary Science Letters*, *263*(1-2), 88–103. https://doi.org/10.1016/j.epsl.2007.09.005

Smith, W. H. (1997). Global seafloor topography from satellite altimetry and ship depth soundings. *Science*, *277*(5334), 1956–1962. https://doi.org/10.1126/science.277.5334.1956

Stierle, E., Vavryčuk, V., Šílený, J., & Bohnhoff, M. (2014). Resolution of non-double-couple components in the seismic moment tensor using regional networks—I: A synthetic case study. *Geophysical Journal International*, *196*(3), 1869–1877. https://doi.org/10.1093/gji/ggt502

Tsai, V. C., Nettles, M., Ekström, G., & Dziewonski, A. M. (2005). Multiple CMT source analysis of the 2004 Sumatra earthquake. *Geophysical Research Letters*, *32*, L17304. https://doi.org/10.1029/2005GL023813

Vavryčuk, V. (2014). Moment tensor decompositions revisited. *Journal of Seismology*, *19*(1), 231–252.

Viete, D. R., Richards, S. W., Lister, G. S., Oliver, G. J. H., & Banks, G. J. (2010). Lithospheric-scale extension during Grampian orogenesis in Scotland. *Geological Society, London, Special Publications*, *335*(1), 121–160. https://doi.org/10.1144/SP335.7

Waldhauser, F., Schaff, D. P., Diehl, T., & Engdahl, E. R. (2012). Splay faults imaged by fluid-driven aftershocks of the 2004 M_w 9.2 Sumatra-Andaman earthquake. *Geology*, *40*(3), 243–246.

Warren, L. M., & Shearer, P. M. (2006). Systematic determination of earthquake rupture directivity and fault planes from analysis of long-period *P*-wave spectra. *Geophysical Journal International*, *164*(1), 46–62. https://doi.org/10.1111/j.1365-246X.2005.02769.x

Weller, O., Lange, D., Tilmann, F., Natawidjaja, D., Rietbrock, A., Collings, R., & Gregory, L. (2012). The structure of the Sumatran fault revealed by local seismicity. *Geophysical Research Letters*, *39*, L01306. https://doi.org/10.1029/2011GL050440

Wells, M. L., Hoisch, T. D., Cruz-Uribe, A. M., & Vervoort, J. D. (2012). Geodynamics of synconvergent extension and tectonic mode switching: Constraints from the Sevier-Laramide orogen. *Tectonics*, *31*, TC1002. https://doi.org/10.1029/2011TC002913